Flavoured Dark Matter in Dark Minimal Flavour Violation

TeVPA 2017, Columbus, Ohio

Monika Blanke, **Simon Kast** | August 7, 2017

KARLSRUHE INSTITUTE OF TECHNOLOGY

Approaches to identify Dark Matter

- Extension of SM motivated by a new idea solving several problems (e.g. SUSY, Axions).
- Study of all kind of higher dimensional effective SM-DM interactions in Effective Field Theory (EFT).
- **Simplified models**: Study phenomenology of specific interactions with limited number of parameters.

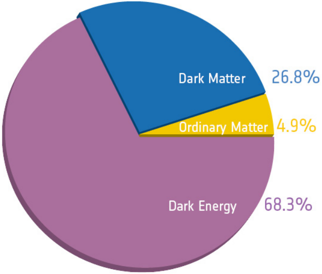

Figure: Energy distribution of the Universe (Planck 2015).

The Flavour Gate to Dark Matter

Assume an analogy to the SM fermions $\rightarrow$ dark flavour triplet χ_i.

The Flavour Gate to Dark Matter

Assume an analogy to the SM fermions $\rightarrow$ dark flavour triplet χ_i.

Flavoured Dark Matter coupling to SM right-handed up-quark triplet: [Blanke, SK, '17]

$$\mathcal{L}_{\text{NP,int}} = -\lambda_{ij}\bar{u}_{Ri}\chi_j\phi + h.c.$$

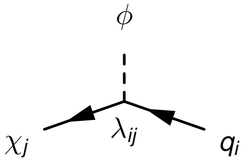

Figure: New physics interaction (basic vertex).

- DM flavour triplet χ_j, Dirac fermion, SM gauge singlet.
- Heavy scalar mediator ϕ, carrying colour and hypercharge.
- Lagrangian has unbroken $\mathbb{Z}_3$ symmetry and hence yields stability of DM χ (for $m_\phi > m_\chi$).

Dark Minimal Flavour Violation

[Agrawal, Blanke, Gemmler '14]

Flavour Symmetry

$$U(3)_u \times U(3)_d \times U(3)_q \times U(3)_\chi$$

is only broken by SM Yukawa couplings and the DM-quark coupling λ_{ij} (Dark Minimal Flavour Violation).

$\Rightarrow$ only DM mass splitting comes from RG running:

$$m_{ij} = m_\chi(\mathbb{1} + \eta\lambda^\dagger\lambda + ...)_{ij}.$$

- η depends on the full theory $\rightarrow$ has to be a parameter of the simplified model.
- flavour with lowest mass is our DM candidate.
  $\rightarrow$ we choose the "top-flavour". [Kilic, Klimek, Yu '15]

Parametrization of DM-Quark Coupling Matrix

After using all the symmetries at our disposal λ has 9 parameters left and can be parametrized as:

$$\lambda = U_{23}^{\lambda} U_{13}^{\lambda} U_{12}^{\lambda} D_{\lambda}$$

- D_λ is a real diagonal matrix $D_\lambda = \text{diag}(D_{\lambda,11}, D_{\lambda,22}, D_{\lambda,33})$.
- U_{ij}^{λ} are unitary matrices with mixing angles Θ_{ij} and phases δ_{ij}.

$\Rightarrow$ new source of flavour <u>and</u> CP violation

How to Detect Flavoured Dark Matter?

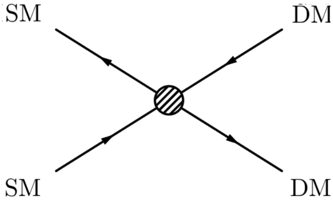

collider searches

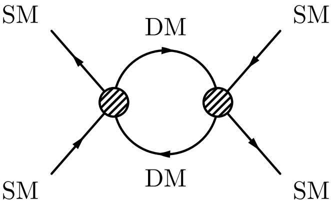

precision flavour data

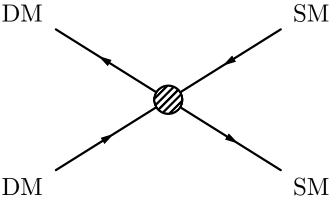

indirect detection / freeze-out

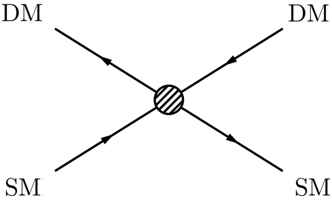

direct detection

Constraints from SUSY Searches at LHC

Constraints from SUSY-searches ($t\bar{t}$ or dijet final states) [ATLAS collaboration '14]

Study $pp \to \phi\phi^\dagger \to q\bar{q}\chi\bar{\chi}$

- Production either through QCD or NP interaction (coupling-dependent).
- Decay either to top or jet ($+ \not{E}_T$).

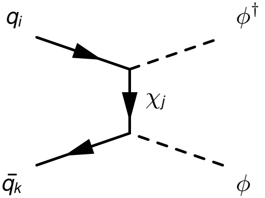

Figure: NP interaction production channel.

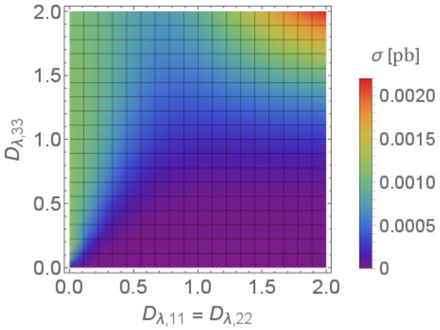

Figure: Cross section for $t\bar{t}$ final state, mixing angles set to zero.

Constraints from SUSY Searches at LHC

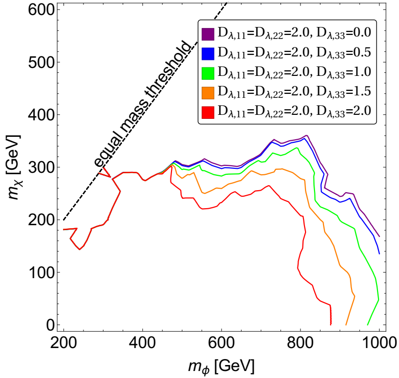

Figure: Exclusion plot for dijet final state, mixing angles set to zero.

- The phenomenologically interesting region is $m_\chi \leq 1$ TeV.
- Too large couplings $D_{\lambda,ii}$ would exclude nearly all of parameterspace.
- Most serious constraints come from dijet final state.

$\Rightarrow$ Safe parameter-space:

$$m_\phi \geq 850 \text{ GeV}$$

$$2.0 \geq D_{\lambda,33} > D_{\lambda,22}, D_{\lambda,11}$$

$\Rightarrow$ Also save with mixings allowed.

Flavour Constraints from Neutral Meson Mixing

- No mesons with top-quark are possible, the only constraints come from D-mesons.
  $\Rightarrow$ not too strong

- The NP contribution has to be smaller than experimental bounds [Heavy Flavor Averaging Group '16].
  $\Rightarrow$ constraints on mixing angles, mostly Θ_{12}

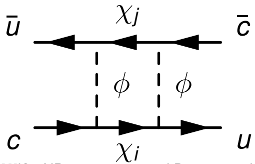

Figure: NP contr. to neutral D-meson mixing.

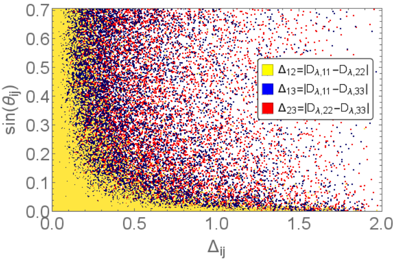

Figure: Valid mixing angles for different coupling splittings. $m_\phi = 850$ GeV and $m_\chi = 250$ GeV.

DM Constraints from Observed Relic Abundance

- Assume DM abundance as a thermal relic.
- Depending on mass-splitting several freeze-out scenarios are possible.
- If DM mass is below top-mass several channels drop out.
  $\Rightarrow$ different impact on parameters
- Annihilation has to be just as large as to produce the correct relic density [Steigman, Dasgupta, Beacom '12].
  $\Rightarrow$ cuts out valid area for $D_{\lambda,ii}$ depending on m_ϕ and m_χ
- Lower bounds on DM mass depending on mediator mass.
- Depending on η an upper DM bound arises in single-flavour freeze-out scenarios.

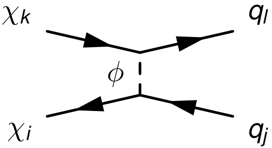

Figure: Annihilation of DM flavours.

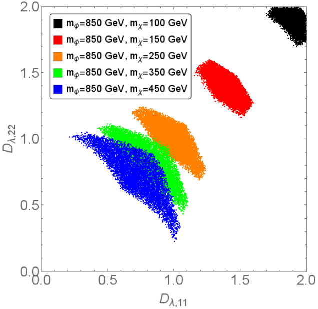

Figure: Valid regions in quasi-degenerate freeze-out scenario.

DM Bounds from Direct Detection Experiments

- Strong exclusion bounds
  [LUX collaboration '16], [XENON1T '17]
- Many contributions to total WIMP-nucleon cross section, only Z-penguin with neutron is negative.
  $\Rightarrow$ saves the day
- Tree level and neutron Z-penguin have to nearly cancel each other.
  $\Rightarrow$ serious constraints on Θ_{13}
- For too large couplings the cancellation is no longer possible $\rightarrow$ excluded.
- Top-flavoured DM is the natural choice.

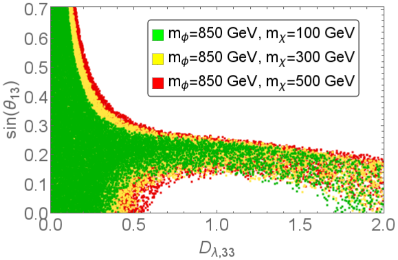

Figure: Valid mixing angle Θ_{13} vs $D_{\lambda,33}$.

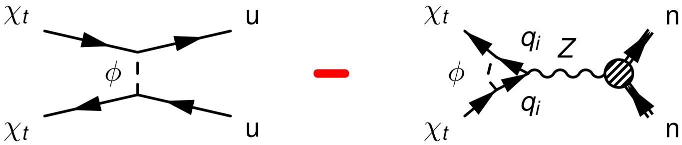

Figure: Cancellation of tree-level and neutron Z-penguin contributions (symbolic).

Combined Analysis of Constraints

- The combination of relic abundance and direct detection constraints confines Θ_{13} to a narrow interval around the “perfect” cancellation point.
- The lower and upper bounds on the DM mass become more serious, since the parameters do not only have to fulfill relic abundance constraints.
- The combined analysis clearly prefers top-flavoured DM.

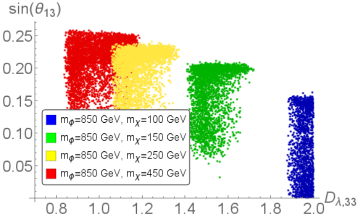

Figure: Valid regions in Θ_{13}-$D_{\lambda,33}$-plane (QDF).

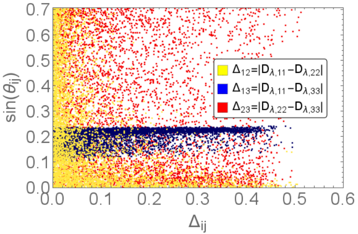

Figure: Valid regions for $m_\phi = 850$ GeV and $m_\chi = 250$ GeV (QDF).

Implications of Enhanced Constraints

Xenon has 9 stable or quasi-stable isotopes (7 make up significant fraction of natural Xenon).

$\Rightarrow$ perfect cancellation in DD CS different for isotopes

$\Rightarrow$ for enhanced constraints not always possible

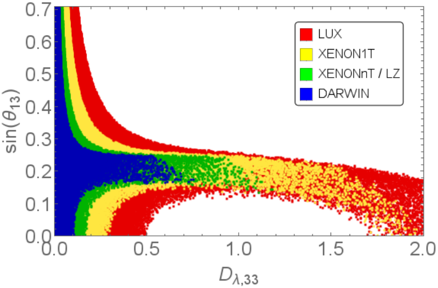

Figure: Valid regions for $m_\phi = 850$ GeV and $m_\chi = 250$ GeV in Θ_{13}-$D_{\lambda,33}$-plane for different strengths of LUX constraints in QDF.

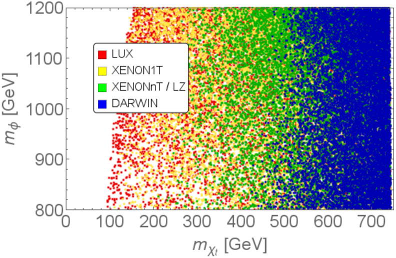

Figure: Valid regions in Mass Scan for different strengths of LUX constraints in QDF.

Conclusion and Outlook

Karlsruhe Institute of Technology

- All kinds of different constraints $\rightarrow$ multitude of effects and interesting interplay.
- Especially interesting effect on mixing angle θ_{13} due to DD and RA constraints.
  $\Rightarrow$ Future measurements of direct detection experiments will test a large part of the parameter space.
  $\Rightarrow$ Ongoing Xenon experiments or experiments with other noble gases well motivated.
- Simplified models are powerful tool to study diversity of constraints.
- Going beyond Minimal Flavour Violation is worth the effort.
  $\rightarrow$ Dark Minimal Flavour Violation as guidance.
- Work in Progress: Coupling dark matter to left-handed $SU(2)$ quark-doublet

[Blanke, Das, SK, in preparation]

References I

- Georges Aad et al. "Search for squarks and gluinos with the ATLAS detector in final states with jets and missing transverse momentum using $\sqrt{s} = 8$ TeV proton–proton collision data". In: *JHEP* 09 (2014), p. 176. DOI: 10.1007/JHEP09(2014)176. arXiv: 1405.7875 [hep-ex].
- Georges Aad et al. "Search for top squark pair production in final states with one isolated lepton, jets, and missing transverse momentum in $\sqrt{s}$ =8 TeV *pp* collisions with the ATLAS detector". In: *JHEP* 11 (2014), p. 118. DOI: 10.1007/JHEP11(2014)118. arXiv: 1407.0583 [hep-ex].
- R. Adam et al. "Planck 2015 results. I. Overview of products and scientific results". In: (2015). arXiv: 1502.01582 [astro-ph.CO].

References II

- Prateek Agrawal, Monika Blanke, and Katrin Gemmler. "Flavored dark matter beyond Minimal Flavor Violation". In: *JHEP* 1410 (2014), p. 72. DOI: 10.1007/JHEP10(2014)072. arXiv: 1405.6709 [hep-ph].
- D. S. Akerib et al. "Results from a search for dark matter in the complete LUX exposure". In: (2016). arXiv: 1608.07648 [astro-ph.CO].
- Y. Amhis et al. "Averages of b-hadron, c-hadron, and τ-lepton properties as of summer 2016". In: (2016). arXiv: 1612.07233 [hep-ex].
- Brian Batell, Josef Pradler, and Michael Spannowsky. "Dark Matter from Minimal Flavor Violation". In: *JHEP* 08 (2011), p. 038. DOI: 10.1007/JHEP08(2011)038. arXiv: 1105.1781 [hep-ph].

References III

- Gianfranco Bertone, Dan Hooper, and Joseph Silk. “Particle dark matter: Evidence, candidates and constraints”. In: *Phys. Rept.* 405 (2005), pp. 279–390. DOI: 10.1016/j.physrep.2004.08.031. arXiv: hep-ph/0404175 [hep-ph].
- Monika Blanke and Simon Kast. “Top-Flavoured Dark Matter in Dark Minimal Flavour Violation”. In: *JHEP* 05 (2017), p. 162. DOI: 10.1007/JHEP05(2017)162. arXiv: 1702.08457 [hep-ph].
- Andrzej J. Buras. “Minimal flavor violation”. In: *Acta Phys. Polon.* B34 (2003), pp. 5615–5668. arXiv: hep-ph/0310208 [hep-ph].

References IV

- G. D'Ambrosio et al. "Minimal flavor violation: An Effective field theory approach". In: *Nucl. Phys.* B645 (2002), pp. 155–187. DOI: 10.1016/S0550-3213(02)00836-2. arXiv: hep-ph/0207036 [hep-ph].
- Sara Diglio. "XENON1T: the start of a new era in the search for Dark Matter". In: *PoS* DSU2015 (2016), p. 032.
- Jonathan L. Feng, Jason Kumar, and David Sanford. "Xenophobic Dark Matter". In: *Phys. Rev.* D88.1 (2013), p. 015021. DOI: 10.1103/PhysRevD.88.015021. arXiv: 1306.2315 [hep-ph].
- Can Kilic, Matthew D. Klimek, and Jiang-Hao Yu. "Signatures of Top Flavored Dark Matter". In: *Phys.Rev.* D91.5 (2015), p. 054036. DOI: 10.1103/PhysRevD.91.054036. arXiv: 1501.02202 [hep-ph].

References V

Gary Steigman, Basudeb Dasgupta, and John F. Beacom. “Precise Relic WIMP Abundance and its Impact on Searches for Dark Matter Annihilation”. In: *Phys.Rev.* D86 (2012), p. 023506. DOI: 10.1103/PhysRevD.86.023506. arXiv: 1204.3622 [hep-ph].

James D. Wells. “Annihilation cross-sections for relic densities in the low velocity limit”. In: (1994). arXiv: hep-ph/9404219 [hep-ph].

Dark Matter Evidence

- 1933: Virial theorem $2T = -U$ applied to coma cluster.

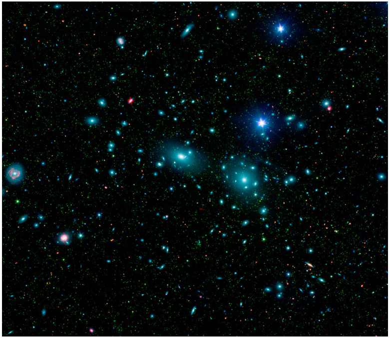

Figure: Coma cluster.

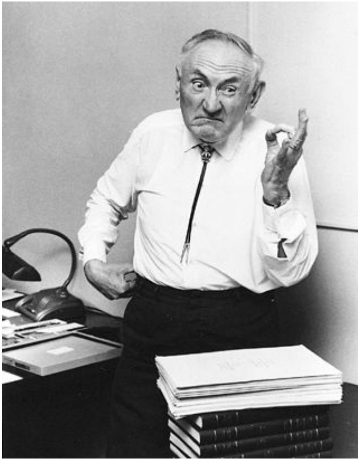

Figure: Fritz Zwicky.

Dark Matter Evidence

- 1970's: Rotation curves of stars in galaxies.

Figure: Vera Rubin.

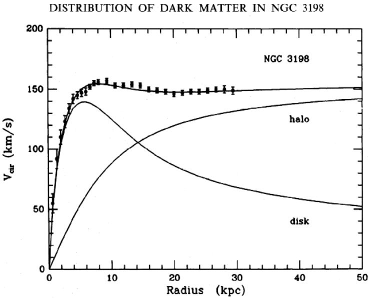

Figure: Rotation curve data vs. predictions.

References

Dark Matter Evidence

- After recombination baryonic structure formation profits from preexisting dense DM regions
  $\Rightarrow$ galaxy formation possible in age of the Universe.

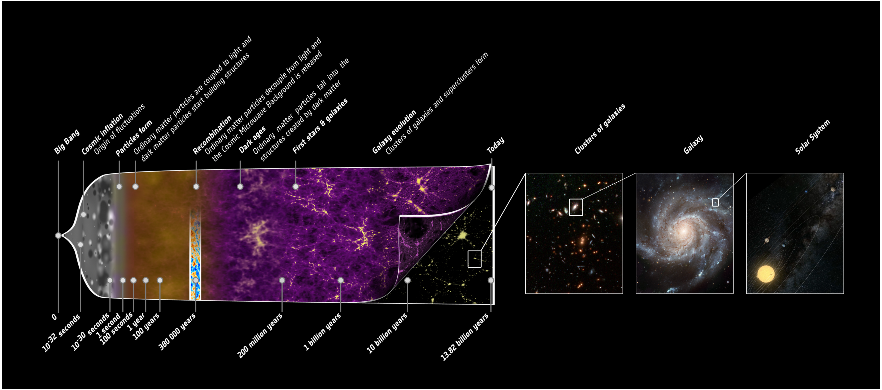

Figure: History of the Universe.

References

Dark Matter Evidence

- Gravitational lensing effects → Bullet Cluster. Misalignment of visible and gravitational mass distribution.

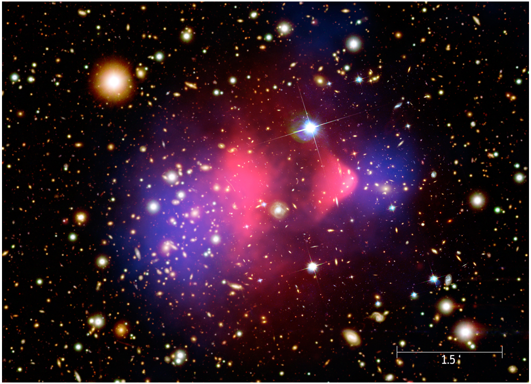

Figure: Bullet cluster. Visible matter distribution (red) and dark matter distribution (blue).

Dark Matter Evidence

- Imprints in Cosmic Microwave Background (CMB).

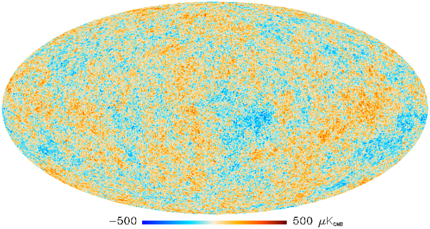

Figure: Temperature fluctuations in CMB (Planck 2013).

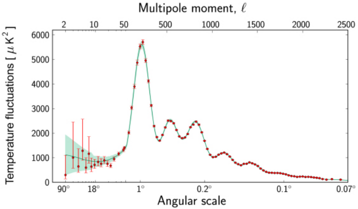

Figure: CMB power spectrum (Planck 2013).

Approaches to identify Dark Matter

- Extension of SM motivated by a new idea solving several problems (e.g. SUSY, Axions).
- Study of all kind of higher dimensional effective SM-DM interactions in Effective Field Theory (EFT).
- **Simplified models**: Study phenomenology of specific interactions with limited number of parameters.

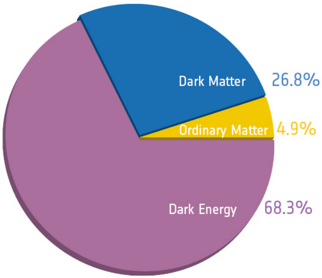

Figure: Energy distribution of the Universe (Planck 2015).

The Flavour Gate to Dark Matter

Karlsruhe Institute of Technology

[Agrawal, Blanke, Gemmler '14]

Assume an analogy to the SM fermions $\rightarrow$ dark flavour triplet χ_i.

The Flavour Gate to Dark Matter

[Agrawal, Blanke, Gemmler '14]

Assume an analogy to the SM fermions $\rightarrow$ dark flavour triplet χ_i.

Flavoured Dark Matter coupling to SM right-handed up-quark triplet:

$$\mathcal{L}_{\text{NP,int}} = -\lambda_{ij} \bar{u}_{Ri} \chi_j \phi + h.c.$$

$$\mathcal{L}_{\text{NP,mass}} = -m_\phi \phi^\dagger \phi - m_\chi \bar{\chi} \chi$$

- DM flavour triplet χ_j, Dirac fermion, SM gauge singlet.
- Heavy scalar mediator ϕ, carrying colour and hypercharge.
- Lagrangian has unbroken $\mathbb{Z}_3$ symmetry and hence yields stability of DM χ (for $m_\phi > m_\chi$).

Dark Minimal Flavour Violation

[Agrawal, Blanke, Gemmler '14]

Flavour Symmetry

$$U(3)_u \times U(3)_d \times U(3)_q \times U(3)_\chi$$

is only broken by SM Yukawa couplings and the DM-quark coupling λ_{ij} (Dark Minimal Flavour Violation).

$\Rightarrow$ Beyond Minimal Flavour Violation.

$\Rightarrow$ only DM mass splitting comes from RG running:

$$m_{ij} = m_\chi(\mathbb{1} + \eta\lambda^\dagger\lambda + ...)_{ij} = m_\chi(1 + \eta(D_{\lambda,ii})^2 + ...)\delta_{ij}.$$

- η depends on the full theory $\rightarrow$ has to be a parameter of the simplified model.
- flavour with lowest mass is our DM candidate.
  $\rightarrow$ we choose the "top-flavour". [Kilic, Klimek, Yu '15]

Parametrization of DM-Quark Coupling Matrix

Dark Minimal Flavour Violation (DMFV): λ_{ij} is a general 3×3 coupling matrix $\rightarrow$ 9 real parameters and 9 complex phases.

- Can be split up as (bilinear diagonalization):

$$\lambda = U^{\lambda} D_{\lambda} V^{\lambda}$$

  with unitary matrices U^{λ}, V^{λ} and diagonal real matrix D_{λ}.
- Use redundancy to eliminate 3 phases in U^{λ}.
- Use flavour symmetry in dark sector $U(3)_{\chi}$ to get rid of V^{λ}

After using all the symmetries at our disposal λ has 9 parameters left and can be parametrized as:

$$\lambda = U_{23}^{\lambda} U_{13}^{\lambda} U_{12}^{\lambda} D_{\lambda}$$

Constraints from SUSY Searches at LHC

[ATLAS collaboration '14]

- Study the process $pp \to \phi\phi^\dagger \to q\bar{q}\chi\bar{\chi}$.
- Depending on decay product of ϕ we detect either a top-signature or a jet ($+\not{E}_T$).
- Inspiration from SUSY searches at LHC
  $\Rightarrow$ Upper bounds on CS of both $t\bar{t}$ and dijet signals.

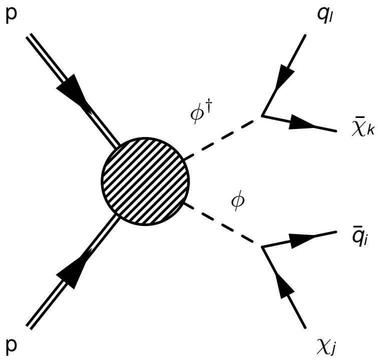

Figure: Studied LHC DM production processes.

Constraints from SUSY Searches at LHC

Involved QCD processes

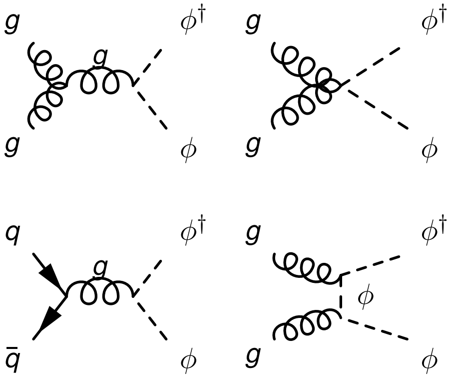

Involved NP processes

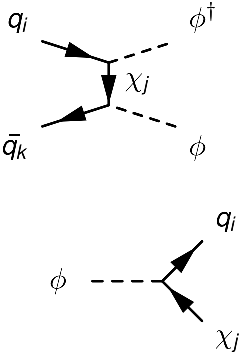

Constraints from $t\bar{t}+\not{E}_T$ Searches at LHC

- $D_{\lambda,33}$ increased
  $\rightarrow$ BR of decay goes up.
- $D_{\lambda,11}$, $D_{\lambda,22}$ increased
  $\rightarrow$ BR of decay goes down.

- **BUT**: For high $D_{\lambda,11} = D_{\lambda,22}$ we observe increasing excluded areas.

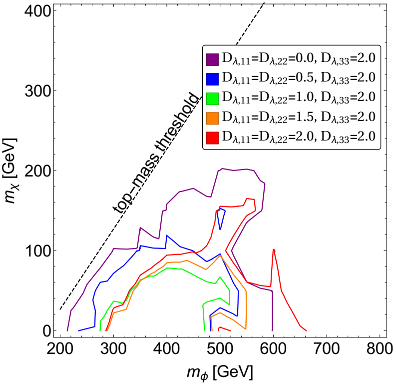

Figure: Exclusion plot for $t\bar{t}$ final state, mixing angles set to zero.

References

Constraints from SUSY Searches at LHC

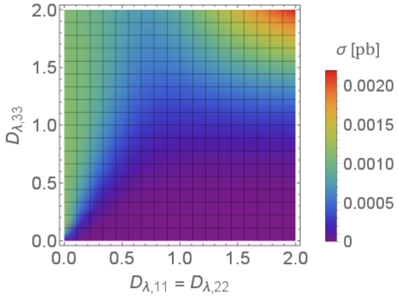

Figure: Cross section of $t\bar{t}$ final state for $m_\phi = 850$ GeV and $m_\chi = 50$ GeV, mixing angles set to zero.

Explanation: NP production

- Major contribution to total production (for high $D_{\lambda,11}$, $D_{\lambda,22}$)
- This effect can make up for drop in BR
- $D_{\lambda,33}$ not relevant, since the protons do not contain top
- Very high couplings can lead to serious exclusion areas.

Constraints from dijet + $\not{E}_T$ Searches at LHC

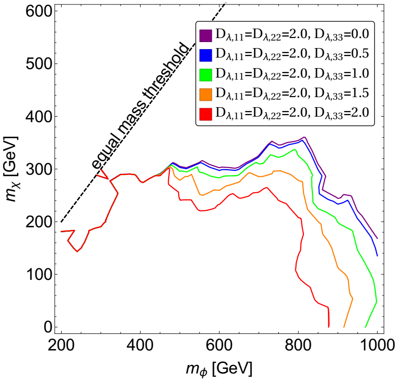

Figure: Exclusion plot for dijet final state, mixing angles set to zero.

- Stronger exclusion bounds on model.
- The phenomenologically interesting region is $m_\chi \lesssim 1$ TeV.
- Too large couplings $D_{\lambda,ii}$ would exclude nearly all of parameter space.
- Most serious constraints come from dijet final state.

$\Rightarrow$ Safe parameter-space:

$$m_\phi \geq 850 \text{ GeV}$$

$$2.0 \geq D_{\lambda,33} \geq D_{\lambda,22}, D_{\lambda,11}$$

Influence of Mixing Angles on LHC production

- Mixing angles shift influences between couplings $D_{\lambda,ii}$.
  $\Rightarrow$ For big splitting in the couplings, mixing angles can cause big shifts in cross sections.
- For our choice of m_ϕ bounds from $t\bar{t}$ final state cause no constraints.
- Worst allowed case for dijet final state, in our safe parameter-space, is $D_{\lambda,11} = D_{\lambda,22} = D_{\lambda,33} = 2.0$
  $\Rightarrow$ Unchanged by mixing angles.

$\Rightarrow$ Mixing angles can cause no problem with this choice of safe parameter-space.

Flavour Constraints from Neutral Meson Mixing

[UTfit collaboration ’14]

- No mesons with top-quark are possible, the only constraints come from D-mesons.
  $\Rightarrow$ not too strong
- The NP contribution has to be smaller than experimental bounds.

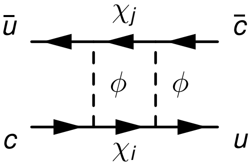

Figure: NP contr. to neutral D-meson mixing.

$$
\begin{aligned}
M_{12}^{D,NP} &= \frac{1}{2m_D} \langle \bar{D}^0 | \mathcal{H}_{eff}^{\Delta C=2,new} | D^0 \rangle^* \\
&= \frac{1}{384\pi^2 m_\phi^2} \sum_{i,j} \lambda_{uj}^* \lambda_{cj} \lambda_{ui}^* \lambda_{ci} \cdot L(x_i, x_j) \cdot \eta_D \cdot m_D f_D^2 \hat{B}_D .
\end{aligned}
$$

References

Flavour Constraints from Neutral Meson Mixing

$$\left((\lambda\lambda^\dagger)_{cu}\right)^2 = \left((U_\lambda D_\lambda D_\lambda^\dagger U_\lambda^\dagger)_{cu}\right)^2$$

- For degeneracy $D_{\lambda,11} = D_{\lambda,22} = D_{\lambda,33}$ the mixing matrices U_{ij}^λ will drop out.

- The higher the splitting $\Delta_{ij} = D_{\lambda,ii} - D_{\lambda,jj}$, the more we will see the constraints on the mixing angle θ_{ij}.

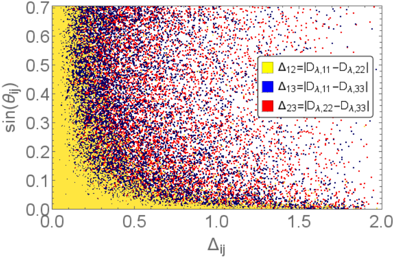

Figure: Valid mixing angles for different coupling splittings. $m_\phi = 850$ GeV and $m_\chi = 250$ GeV.

$\Rightarrow$ Most significant constraints on θ_{12}, other mixings nearly unconstrained.

References

DM Constraints from Observed Relic Abundance

[Steigman, Dasgupta, Beacom '12]

- Assume DM abundance as a thermal relic, $T_f \propto \frac{m_\chi}{20}$
- Annihilation CS has to be just large enough to produce the correct relic density (we allow for a 10% tolerance interval):

$$\langle \sigma v \rangle_{eff,exp} = 2.2 \times 10^{-26} \mathrm{cm}^3/\mathrm{s}.$$

$\Rightarrow$ cuts out valid area for $D_{\lambda,ii}$ depending on m_ϕ and m_χ

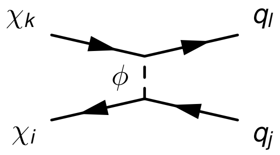

Figure: Annihilation of DM flavours.

$$\langle \sigma v \rangle_{eff} = \frac{1}{9} \times \frac{3}{256\pi} \sum_{i,j=1,2,3} \sum_{k,l=u,c,t} \lambda_{ki}\lambda_{ki}^*\lambda_{lj}\lambda_{lj}^* \frac{\sqrt{\left(4m_\chi^2 - (m_k - m_l)^2\right)\left(4m_\chi^2 - (m_k + m_l)^2\right)}}{\left(m_\phi^2 + m_\chi^2 - \frac{m_k^2}{2} - \frac{m_l^2}{2}\right)^2}.$$

References

DM Constraints from Observed Relic Abundance

- Depending on the mass splitting of the different DM flavours several freeze-out scenarios are possible.

$$m_{ij} = m_\chi(1 + \eta(D_{\lambda,ii})^2 + ...)\delta_{ij}.$$

- For a DM mass below the top-quark mass this decay channel drops out.

  $\Rightarrow$ CS formula and hence impact on parameters can be quite different

- Extreme example: only χ_t present at freeze-out with DM mass below top mass threshold:

$$\langle \sigma v \rangle_{eff} = \frac{3}{256\pi} \sum_{k,l=u,c} \lambda_{k3}\lambda^*_{k3}\lambda_{l3}\lambda^*_{l3} \frac{4m_\chi^2}{\left(m_\phi^2 + m_\chi^2\right)^2}.$$

Quasi-Degenerate Freeze-Out (QDF) Szenario

- All DM flavours are present at the freeze-out.
- We require the mass splitting to be less than 1% (significantly smaller than T_f) for this to happen.
- η is free parameter $\rightarrow$ choose it favourable: -0.01.
- This guarantees top-flavoured DM (see direct detection section for motivation).
- Constraint cuts out valid area for $D_{\lambda,ii}$ depending on m_ϕ and m_χ.
- Lower bound on m_χ due to upper limits for $D_{\lambda,ii}$, depending on m_ϕ.

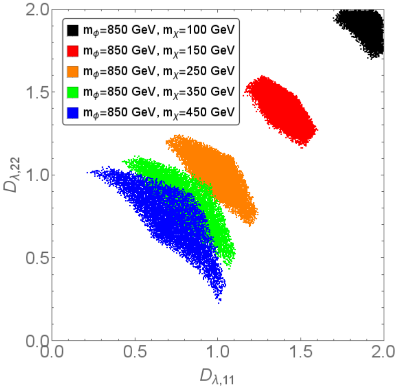

Figure: Valid regions in quasi-degenerate freeze-out scenario.

References

Single Flavour Freeze-Out (SFF) Szenario

- Only m_χ present at freeze-out.
- We require the mass splitting to be more than 10% (significantly bigger than T_f) for this to happen.
- η is free parameter $\rightarrow$ choose it favourable: -0.075.
- This guarantees top-flavoured DM (see direct detection section for motivation).
- Constraint cuts out valid area of parameters depending on m_ϕ and m_χ, with significant effect on mixing angles.
- In addition to lower bound, we also find an upper bound on m_χ due to upper and lower (from mass splitting condition) limits for $D_{\lambda,ii}$, depending on m_ϕ.

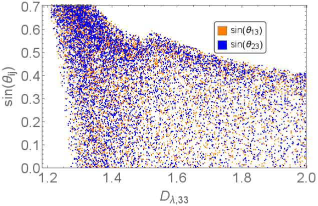

Figure: Valid regions in single flavour freeze-out scenario for $m_\phi = 850$ GeV and $m_\chi = 210$ GeV.

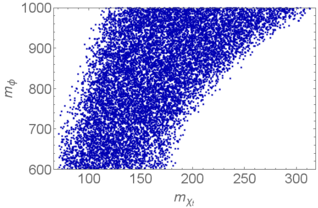

Figure: Mass bounds in single flavour freeze-out scenario.

DM Bounds from Direct Detection Experiments

Many contributions to total WIMP-nucleon cross section:

$$\sigma_n^{SI} = \frac{\mu_n^2}{\pi A^2}|Zf_p + (A-Z)f_n|^2.$$

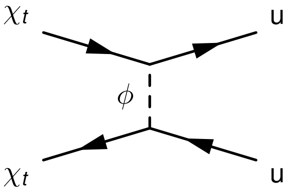

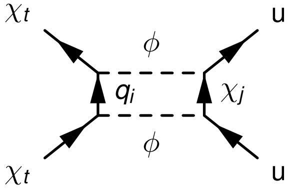

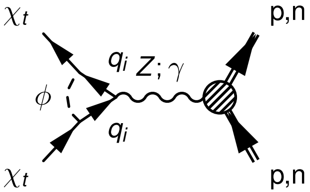

DM Bounds from Direct Detection Experiments

$$f_p^{tree} = 2f_n^{tree} = \frac{|\lambda_{ut}|^2}{4m_\phi^2}.$$

$$f_p^{box} = 2f_n^{box} = \sum_{i,j} \frac{|\lambda_{ui}|^2|\lambda_{jt}|^2}{32\pi^2 m_\phi^2} F\left(\frac{m_{q_i}^2}{m_\phi^2}, \frac{m_{\chi_j}^2}{m_\phi^2}\right).$$

$$f_p^{photon} = -\sum_i \frac{|\lambda_{it}|^2 e^2}{48\pi^2 m_\phi^2}\left(\frac{3}{2} + log\left(\frac{m_{q_i}^2}{m_\phi^2}\right)\right).$$

$$f_p^Z = -\sum_i \frac{3|\lambda_{it}|^2 e^2\left(\frac{1}{2} - 2sin^2(\Theta_W)\right)}{32\pi^2 sin^2(\Theta_W)cos^2(\Theta_W)m_Z^2}\frac{m_{q_i}^2}{m_\phi^2}\left(1 + log\left(\frac{m_{q_i}^2}{m_\phi^2}\right)\right).$$

$$f_n^Z = -\sum_i \frac{3|\lambda_{it}|^2 e^2\left(-\frac{1}{2}\right)}{32\pi^2 sin^2(\Theta_W)cos^2(\Theta_W)m_Z^2}\frac{m_{q_i}^2}{m_\phi^2}\left(1 + log\left(\frac{m_{q_i}^2}{m_\phi^2}\right)\right).$$

DM Bounds from Direct Detection Experiments

[LUX collaboration '15]

- All contributions have to combine to a WIMP-nucleon cross-section below the LUX bounds.
- All contributions are positive, only the Z-penguin with the neutron is negative $\Rightarrow$ saves the day.
- Largest contribution comes from tree-level process. Largest negative term is hence interference term of tree-level and neutron Z-penguin.
- Most important terms, have to nearly cancel each other:

$$A_{\mathcal{I}} \cdot D^4_{\lambda,33} \cdot sin(\theta_{13})^4 - A_{\mathcal{I}\mathcal{I}} \cdot D^4_{\lambda,33} \cdot sin(\theta_{13})^2 \cdot cos(\theta_{13})^2 \cdot cos(\theta_{23})^2$$

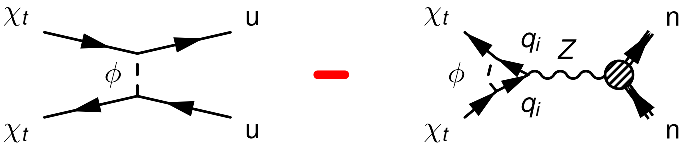

Figure: Cancellation of tree-level and neutron Z-penguin contributions (symbolic).

DM Bounds from Direct Detection Experiments

- Tree level and neutron Z-penguin have to nearly cancel each other.
  $\Rightarrow$ serious constraints on θ_{13}
- For higher couplings the cancellation gets more complicated.
- For too large couplings the cancellation is no longer possible at all
  $\rightarrow$ excluded.
- Top-flavoured DM is the natural choice:
  $\Rightarrow$ Tree-level contribution small
  $\Rightarrow$ Neutron Z-penguin contribution large.

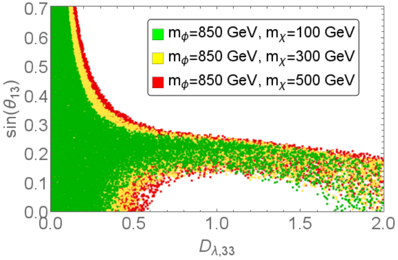

Figure: Valid mixing angle Θ_{13} vs $D_{\lambda,33}$.

Combined Analysis of Constraints (QDF)

Combined application of both flavour, relic abundance and direct detection constraint in quasi-degenerate freeze-out scenario.

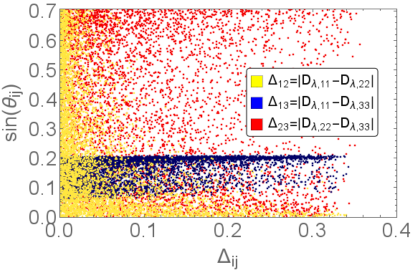

Figure: Valid regions for $m_\phi = 850$ GeV and $m_\chi = 150$ GeV (QDF).

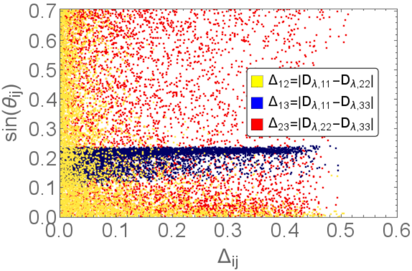

Figure: Valid region for $m_\phi = 850$ GeV and $m_\chi = 250$ GeV (QDF).

Combined Analysis of Constraints (QDF)

- A combination of relic abundance and direct detection constraints confine θ_{13} to a narrow interval.
- The bounds on the DM mass become more serious, since the parameters do not only have to fulfill relic abundance constraints.
- The combined analysis clearly prefers top-flavoured DM.

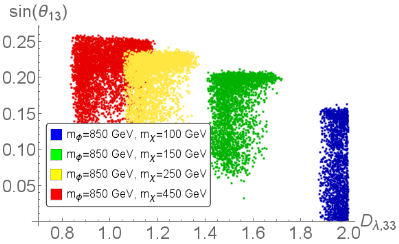

Figure: Valid regions in θ_{13}-$D_{\lambda,33}$-plane (QDF).

Combined Analysis of Constraints (SFF)

Combined application of both flavour, relic abundance and direct detection constraint in single flavour freeze-out scenario.

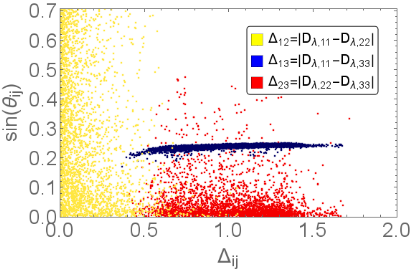

Figure: Valid region for $m_\phi = 850$ GeV and $m_\chi = 225$ GeV (SFF).

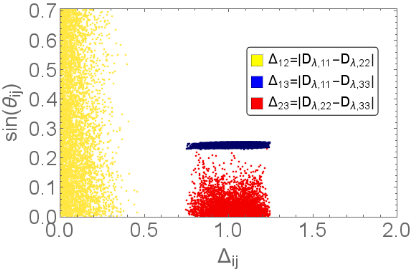

Figure: Valid regions for $m_\phi = 850$ GeV and $m_\chi = 250$ GeV (SFF).

Combined Analysis of Constraints (SFF)

- A combination of relic abundance and direct detection constraints confine θ_{13} to a narrow interval (even more serious than in QDF).
- Especially in SFF the combination of all constraints extremely limits the chance of finding a valid configuration of all parameters for $m_{\chi_t} \leq m_{top}$.
- The combined analysis clearly prefers top-flavoured DM.

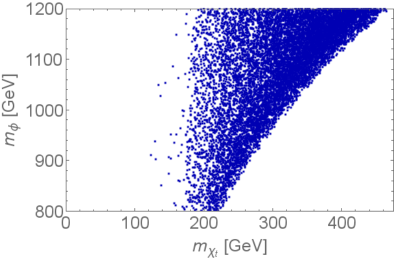

Figure: Valid regions in mass plot for combined constraints (SFF).

Implications of Enhanced Constraints

Xenon has 9 stable or quasi-stable isotopes (7 make up significant fraction of natural Xenon).
$\Rightarrow$ perfect cancellation in DD CS different for isotopes
$\Rightarrow$ for enhanced constraints not always possible

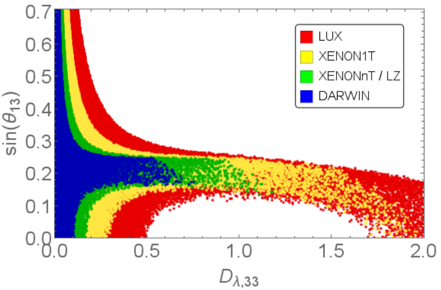

Figure: Valid regions for $m_\phi = 850$ GeV and $m_\chi = 250$ GeV in Θ_{13}-$D_{\lambda,33}$-plane for different strengths of LUX constraints in QDF.

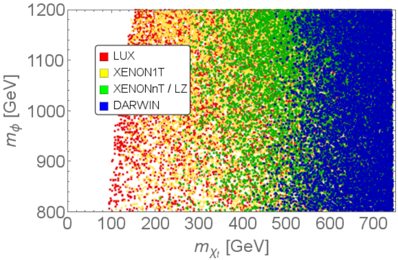

Figure: Valid regions in Mass Scan for different strengths of LUX constraints in QDF.

References

Backup Material 1

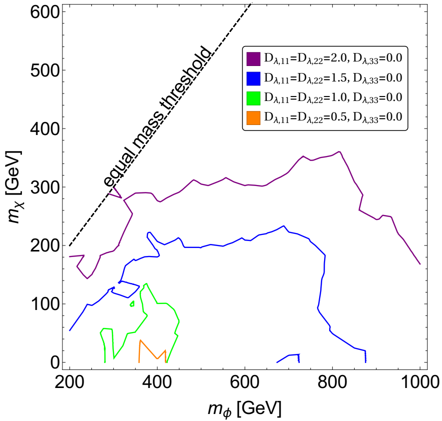

Figure: Exclusion plots for dijet final state for various couplings, mixing angles set to zero.

Backup Material 2

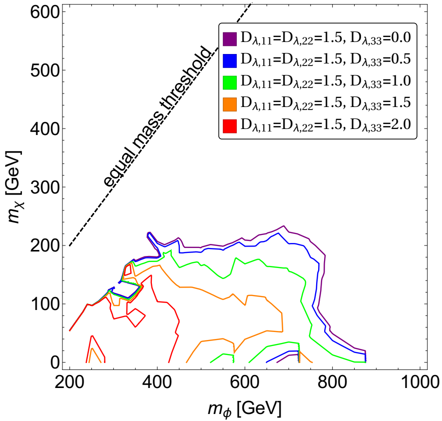

Figure: Exclusion plots for dijet final state for various couplings, mixing angles set to zero.

References

Backup Material 3

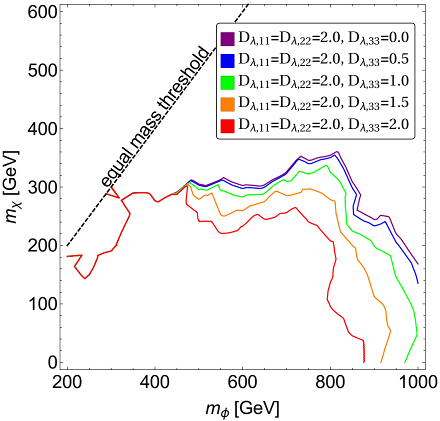

Figure: Exclusion plots for dijet final state for various couplings, mixing angles set to zero.

Backup Material 4

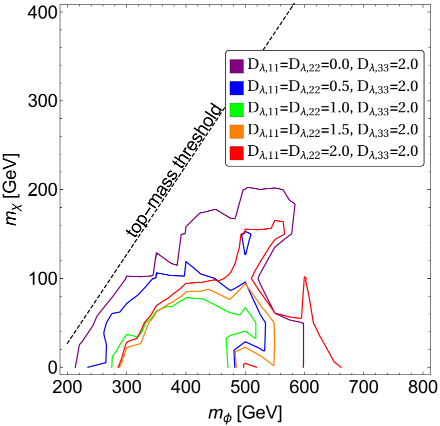

Figure: Exclusion plots for $t\bar{t}$ final state for various couplings, mixing angles set to zero.

Backup Material 5a

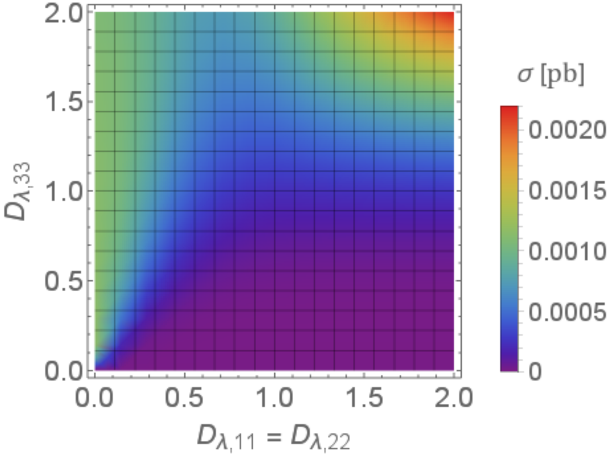

Figure: Cross section for $t\bar{t}$ final state, mixing angles set to zero.

Backup Material 5b

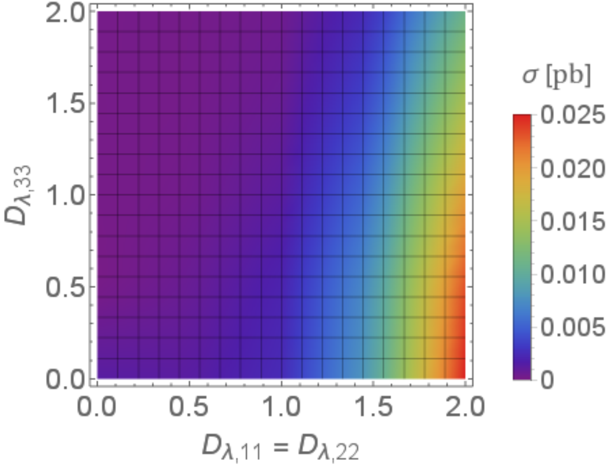

Figure: Cross section for dijet final state, mixing angles set to zero.

Backup Material 6

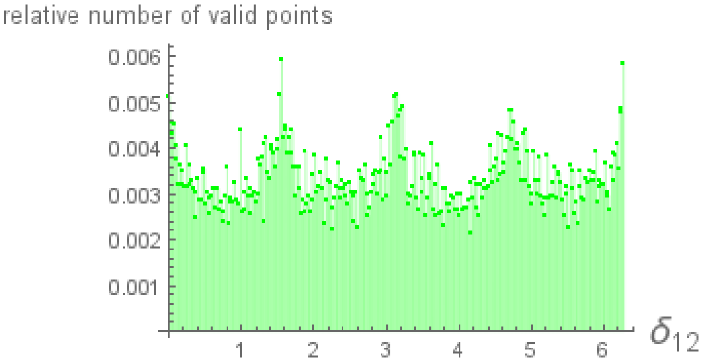

Figure: Impact of flavour constraints on Θ_{12}.

Backup Material 7

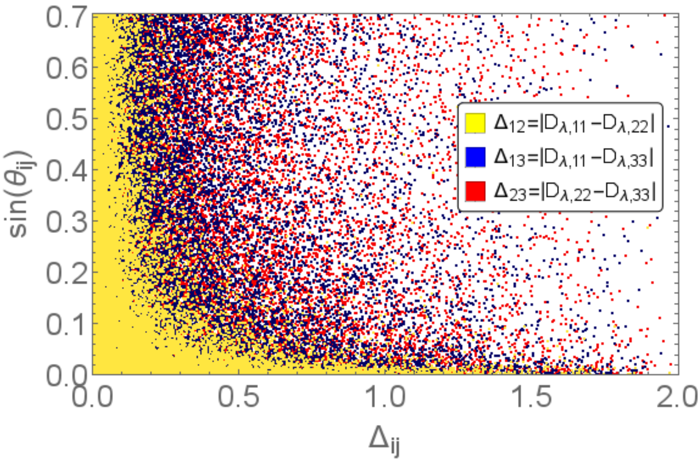

Figure: Valid mixing angles for different coupling splittings. $m_\phi = 850$ GeV and $m_\chi = 250$ GeV.

Backup Material 8

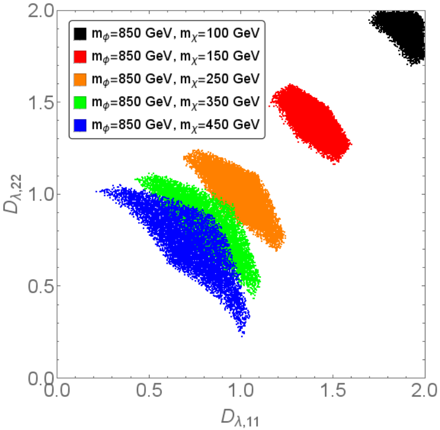

Figure: Valid regions in quasi-degenerate freeze-out scenario in $D_{\lambda,11} - D_{\lambda,22}$-plane for various DM masses.

Backup Material 9

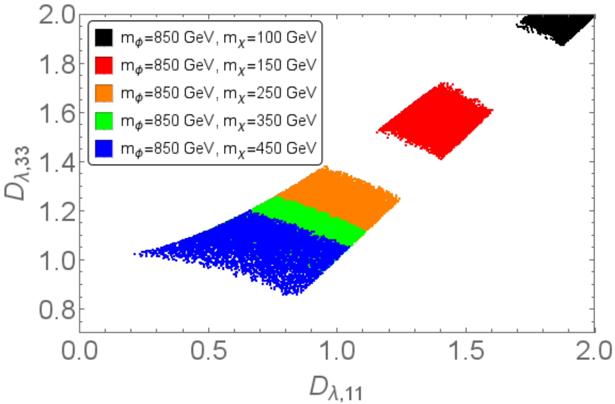

Figure: Valid regions in quasi-degenerate freeze-out scenario in $D_{\lambda,11} - D_{\lambda,33}$-plane for various DM masses.

Backup Material 10

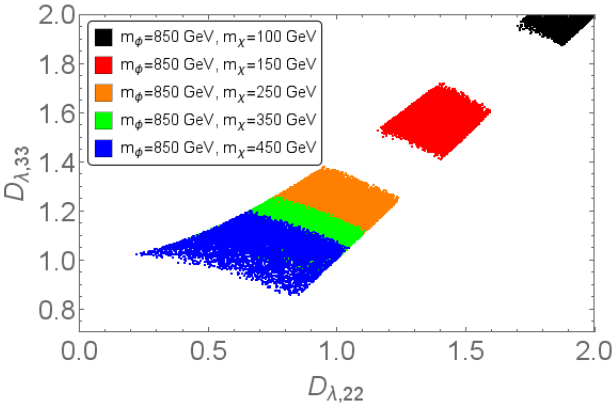

Figure: Valid regions in quasi-degenerate freeze-out scenario in $D_{\lambda,22} - D_{\lambda,33}$-plane for various DM masses.

Backup Material 11

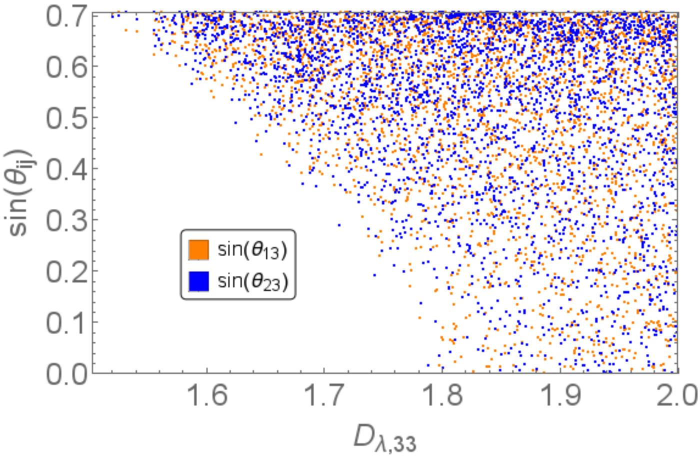

Figure: Valid regions in single-flavour freeze-out scenario in $D_{\lambda,33} - \sin(\Theta_{ij})$-plane for $m_\phi = 850$ GeV and $m_\chi = 150$ GeV.

Backup Material 12

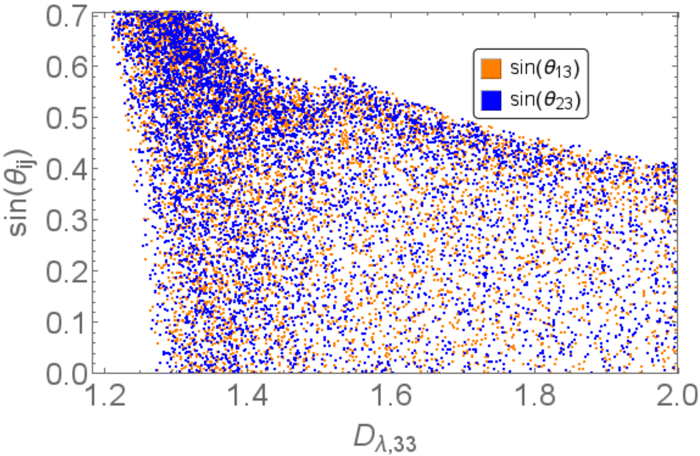

Figure: Valid regions in single-flavour freeze-out scenario in $D_{\lambda,33} - \sin(\Theta_{ij})$-plane for $m_\phi = 850$ GeV and $m_\chi = 210$ GeV.

Backup Material 13

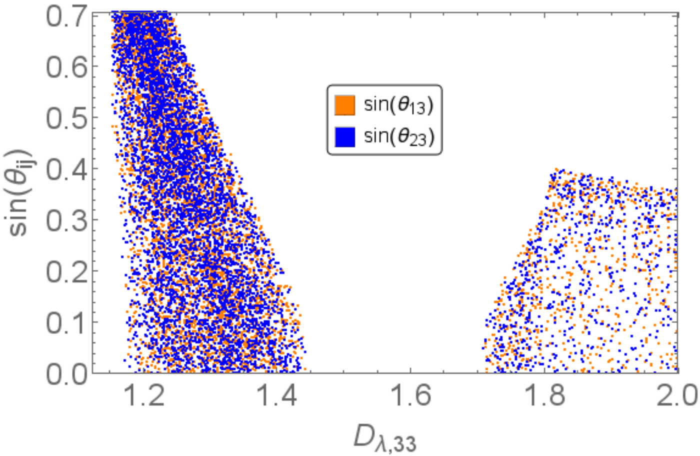

Figure: Valid regions in single-flavour freeze-out scenario in $D_{\lambda,33} - \sin(\Theta_{ij})$-plane for $m_\phi = 850$ GeV and $m_\chi = 230$ GeV.

Backup Material 14

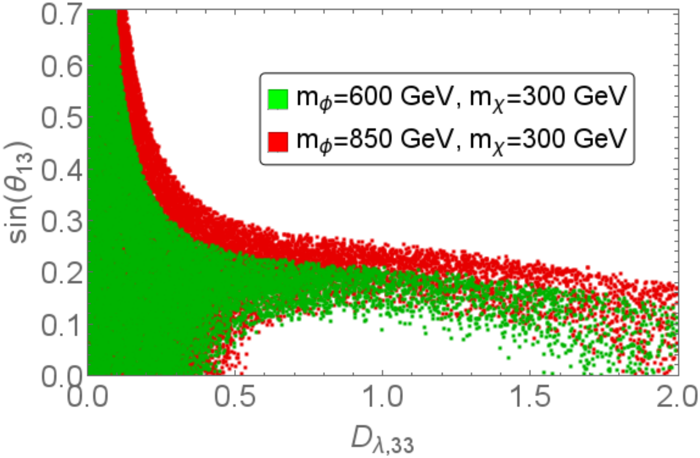

Figure: Valid regions for LUX bounds in $D_{\lambda,33} - \sin(\Theta_{13})-$plane.

Backup Material 15

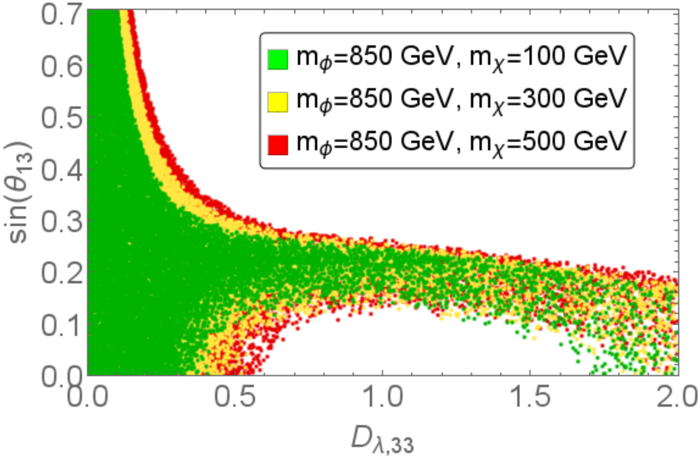

Figure: Valid regions for LUX bounds in $D_{\lambda,33} - \sin(\Theta_{13})-$plane.

Backup Material 16

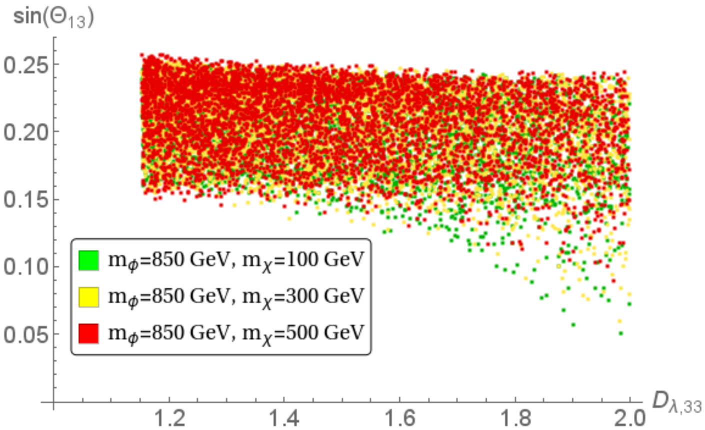

Figure: Valid regions for LUX bounds in $D_{\lambda,33} - \sin(\Theta_{13})-$plane, with SFF splitting applied.

Backup Material 17

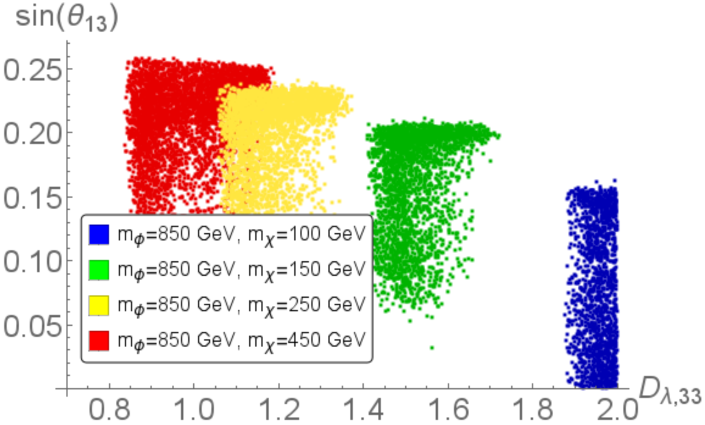

Figure: Valid regions of combined analysis for quasi-degenerate freeze-out scenario in $D_{\lambda,33} - \sin(\Theta_{13})-$plane for different DM masses.

Backup Material 18

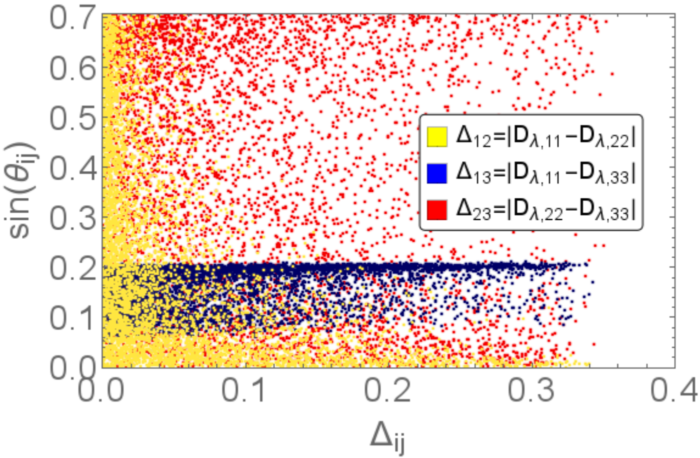

Figure: Valid mixing angles for different coupling splittings for quasi-degenerate freeze-out scenario. $m_\phi = 850$ GeV and $m_\chi = 150$ GeV.

Backup Material 19

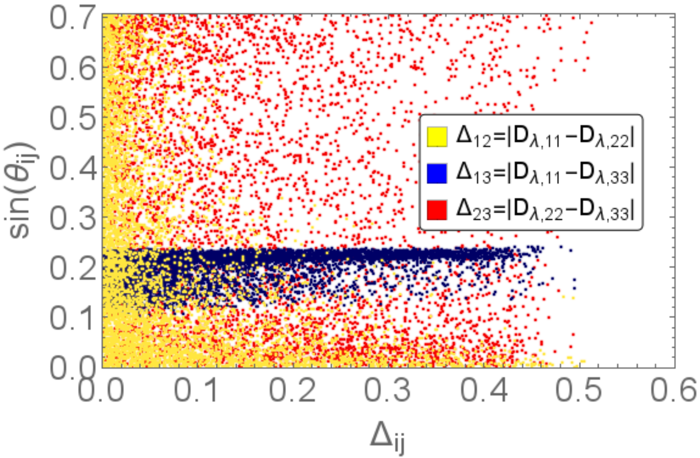

Figure: Valid mixing angles for different coupling splittings for quasi-degenerate freeze-out scenario. $m_\phi = 850$ GeV and $m_\chi = 250$ GeV.

Backup Material 20

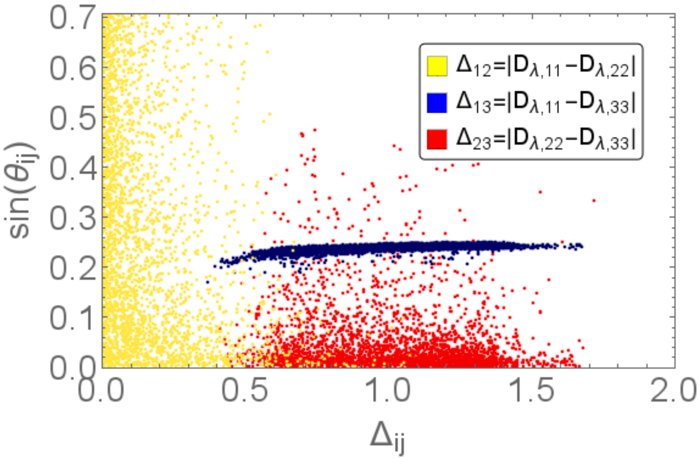

Figure: Valid mixing angles for different coupling splittings for single-flavour freeze-out scenario. $m_\phi = 850$ GeV and $m_\chi = 225$ GeV.

Backup Material 21

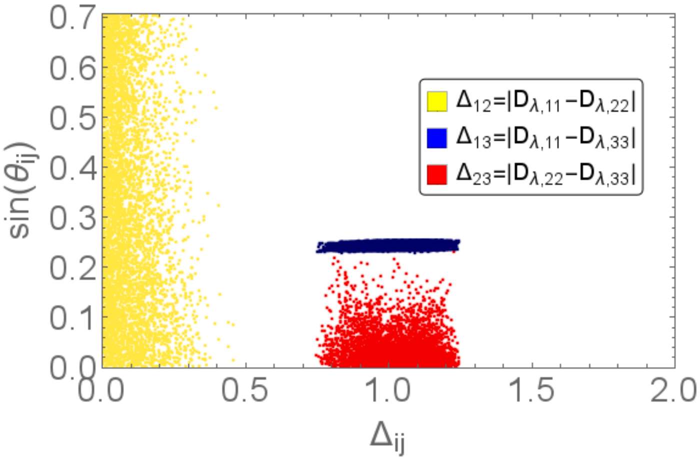

Figure: Valid mixing angles for different coupling splittings for single-flavour freeze-out scenario. $m_\phi = 850$ GeV and $m_\chi = 250$ GeV.

Backup Material 22

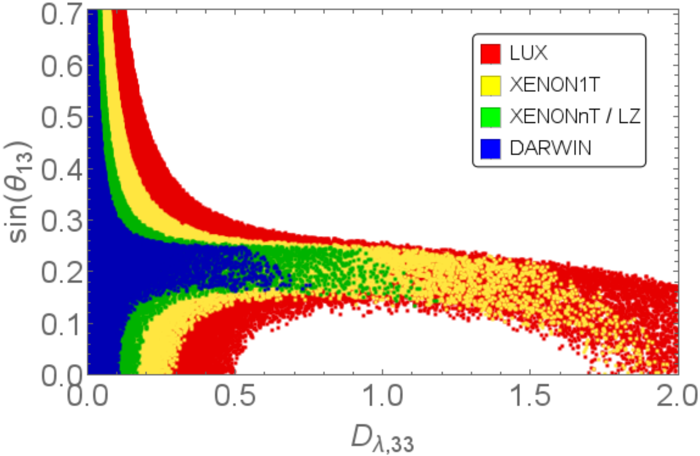

Figure: Valid regions for $m_\phi = 850$ GeV and $m_\chi = 250$ GeV in Θ_{13}-$D_{\lambda,33}$-plane for different strengths of direct detection constraints in QDF.

Backup Material 23

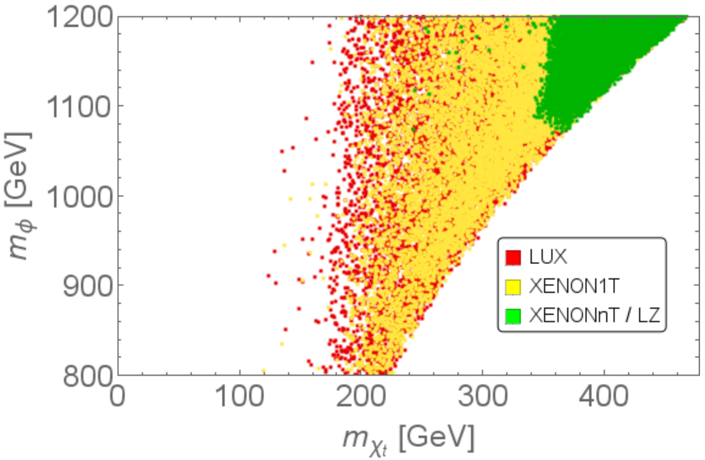

Figure: Valid regions in Mass Scan for different strengths of direct detection constraints in SFF.

Backup Material 24

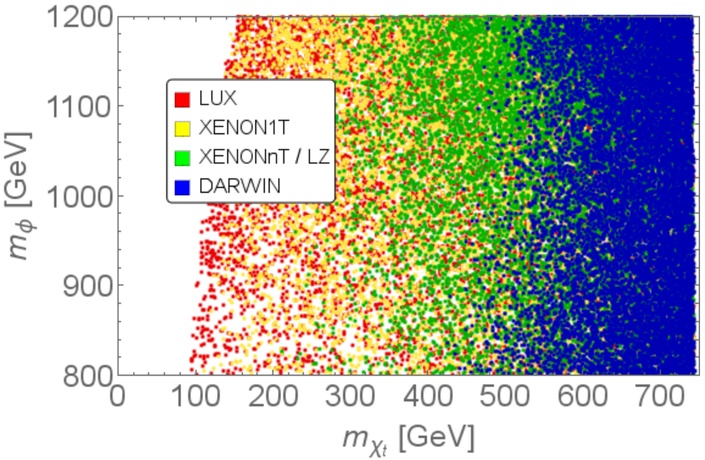

Figure: Valid regions in Mass Scan for different strengths of direct detection constraints in QDF.